STUDIA UBB CHEMIA, LVI, 1, 2011

ELECTROCHEMICAL BEHAVIOUR OF $YBaCo_4O_7$ IN NEUTRAL AQUEOUS SOLUTION

MIRCEA DAN*[a], NICOLAE VASZILCSIN[a], ANDREA KELLENBERGER[a], NARCIS DUTEANU[a]

ABSTRACT. Considering the possibility to use $YBaCo_4O_7$ as oxygen sensor in different environments, the study of electrochemical behaviour of this compound was extended for neutral aqueous solution. Cyclic voltammetry and electrochemical impedance spectroscopy have shown that the compound behaviour in neutral solution is different than that in alkaline one. Compound porosity was determined using BET technique and the results are in accordance with thermogravimetric studies carried out in oxygen flow for $YBaCo_4O_7$ compound, emphasizing the oxygen intake / release by $YBaCo_4O_7$. Correlating all these results, an electrochemical mechanism for $YBaCo_4O_7$ oxidation in neutral aqueous solution has been proposed.

***Keywords*:** *mixed oxides, $YBaCo_4O_7$, electrochemical behaviour of $YBaCo_4O_7$, cyclic voltammetry, electrochemical impedance spectroscopy, BET technique.*

INTRODUCTION

Recent studies have revealed special structural, electrical and magnetic properties of Y-114 mixed cobalt oxide. Due to these properties the mixed cobalt oxides can be used as membranes with high oxygen permeability, oxygen sensors and also as cathodic material in fuel cells [1-5].

The compound $YBaCo_4O_7$, also named Y-114, has been extensively studied since 2002 by Valldor et al. [6,7].

The electrochemical behaviour of Y-114 mixed oxide has been studied in alkaline solutions [8] and had as starting point the electrochemical intercalation the oxygen inside of transitional metal oxide network, presented by J.C. Grenier et al. [9,10] as well as the experimental results regarding the electrochemical cobalt behaviour studied by cyclic voltammetry and electrochemical impedance spectroscopy [11].

The aim of the present paper is to study the electrochemical behaviour of Y-114 mixed oxide in neutral aqueous solution (Na_2SO_4 0.5 mol L^{-1}) and to give an insight of its anodic oxidation mechanism. To the best of our knowledge, there are no studies devoted to the electrochemical behaviour of $YBaCo_4O_7$ in aqueous neutral solutions.

[a] *University "POLITEHNICA", Faculty of Industrial Chemistry and Environmental Engineering, P-ta Victoriei, Nr.6, RO- 300006 Timisoara, Romania, * mircea.dan@chim.upt.ro*

RESULTS AND DISCUSSION

Due to Y-114 structural and morphological complexity, the shape of polarization curves depends on the working conditions; a critical parameter is represented by the polarization rate.

Cyclic voltammograms recorded starting from -1.8 V versus Ag/AgCl are depicted in Fig. 1. All these curves were recorded after a prior polarization at -1.8 V (versus Ag/AgCl) for 300 seconds in order to remove the superficial adsorbed oxygen.

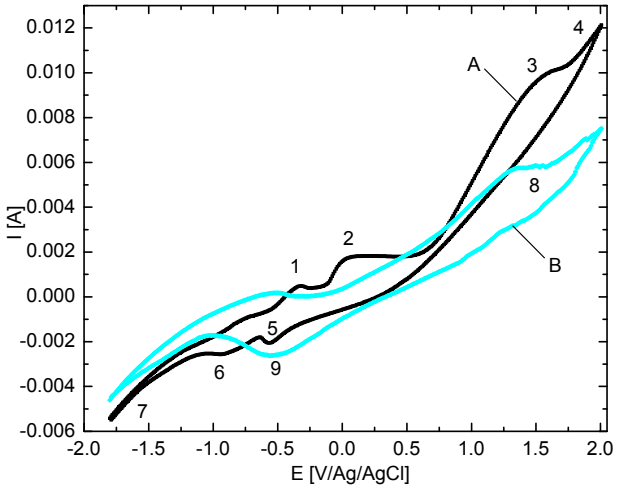

Figure 1. Cyclic voltammograms (A-first cycle; B-fifth cycle) on $YBaCo_4O_7$ working electrode in 0.5 mol L^{-1} Na_2SO_4 solution at 10 mV s^{-1} scan rate.

Analyzing the voltammograms presented in Fig. 1, one can observe the appearance of an anodic peak (1) in the first cycle. This peak can be associated with oxidation of superficial adsorbed hydrogen or of absorbed hydrogen inside the mixed oxide network during cathodic polarization. At more positive electrode potential an anodic wave (2) appears. This wave is associated with cobalt oxidation ($Co \rightarrow Co^{II} + 2e^-$). When the electrode potential becomes more positive a second anodic wave (3) associated with oxidation of Co (II) ions ($Co^{II} \rightarrow Co^{III} + e^-$) can be observed. Like in alkaline media, anodic oxidation of Co (II) ions consists in oxygen insertion into the mixed oxide crystalline structure. When the electrode potential is over 1.17 V versus Ag/AgCl oxygen evolution on electrode surface can be noticed.

On the backward scan a cathodic peak (5) associated with reduction of Co (III) ions to Co (II) ions was noticed, followed by a small current plateau (6) associated with reduction of Co (II) ions to Co. When the electrode potential becomes more negative the hydrogen evolution reaction was observed (7).

The insertion of oxygen ions into the Y-114 crystalline structure leads to its compaction, resulting in the inhibition of redox processes at the Y-114 / electrolyte solution interface. Therefore, the peak height and also the limiting currents decrease during electrochemical polarization. In the fifth cycle, the polarization curves details are fading, except the anodic wave (8) associated with oxidation of Co (II) ions and also the reduction peak (9) associated with the reduction of Co (III) ions to Co (II).

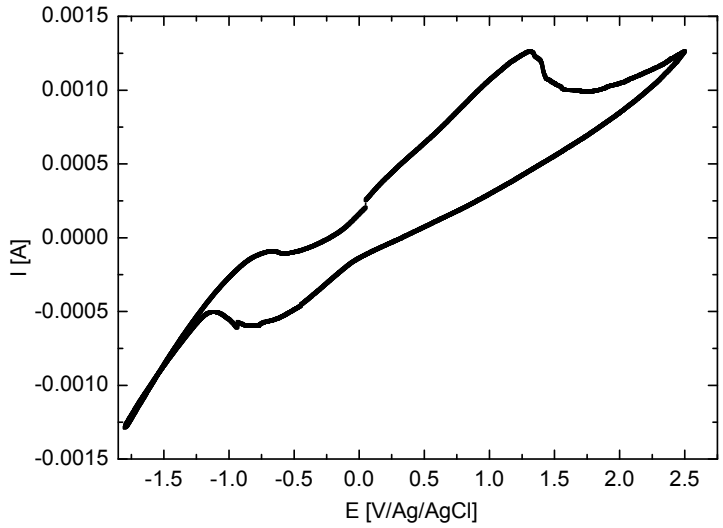

Figure 2. Cyclic voltammogram on $YBaCo_4O_7$ working electrode in 0.5 mol L^{-1} Na_2SO_4 solution at 5 mV s^{-1} scan rate.

When the cyclic voltammograms were recorded at lower polarization rate (5 mV s^{-1}), starting from open circuit potential (OCP) with polarization at OCP for 300 s (Fig. 2), the first peak 1 (Fig. 1) corresponding to the oxidation of Co to Co (II) was not obtained. The lower polarization rate, leads to higher quantities of electricity crossing the interface during the experiment. A further analysis of the CV shown in Fig. 2, reveals a net oxidation peak related to the oxidation of Co (II) ions to Co (III) ions, instead of the plateau recorded at higher polarization speed (Fig. 1). This process is controlled by the diffusion of O^{2-} ions inside of Y-114 mixed oxide and not by the diffusion of different ionic species presented in the adjacent electrolyte solution. Quasi-irreversible nature of the oxidation of Co (II) ions is distinguishable both by the higher difference between potentials related with the oxidation and reduction peak potentials and also by the attenuation with almost 50% of the reduction peak height in comparison with the oxidation peak.

When cyclic voltammograms were recorded at higher polarization scan rate (100 mV s^{-1}) the anodic wave associated with the oxidation of the Co (II) ions is indistinct and overlapped over the oxygen evolution curve as is depicted in Fig. 3.

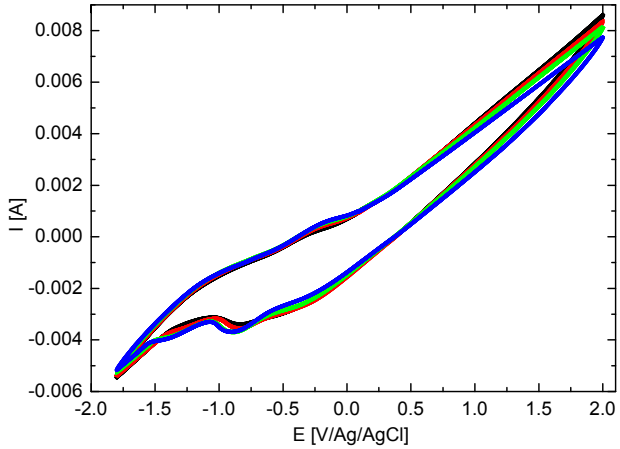

Figure 3. Cyclic voltammogram (5 cycles) on $YBaCo_4O_7$ working electrode in 0.5 mol L^{-1} Na_2SO_4 solution at 100 mV s^{-1} scan rate.

The compound porosity was determined by the BET technique and the results are presented in Table 1.

Table 1. BET surface area, pore diameter, and pore volume of the $YBaCo_4O_7$ sample

Parameter	Value
BET Surface Area	0.3108 m^2 g^{-1}
BJH Desorption average pore diameter (4V/A)	11.0584 nm
BJH Desorption cumulative volume of pores between 1.7000 nm and 300.0000 nm diameter	0.000786 cm^3 g^{-1}

This will lead to large specific surface and provide channels favouring adsorption and desorption of oxygen in time of electrochemical polarization. Compared with dense bulk sample, this porous balls show fast oxygen adsorption and desorption rates.

SEM images obtained for $YBaCo_4O_7$ bar electrode used in this work are presented in Fig. 4. Analyzing the SEM images, a porous structure due to crystallites agglomeration can be observed. This structure equalizes with a large number of pores inside of ceramic electrode. Large pores amount lead to a higher specific surface with channels which favour oxygen adsorption / desorption process and lead to a high concentration of superficial active ions.

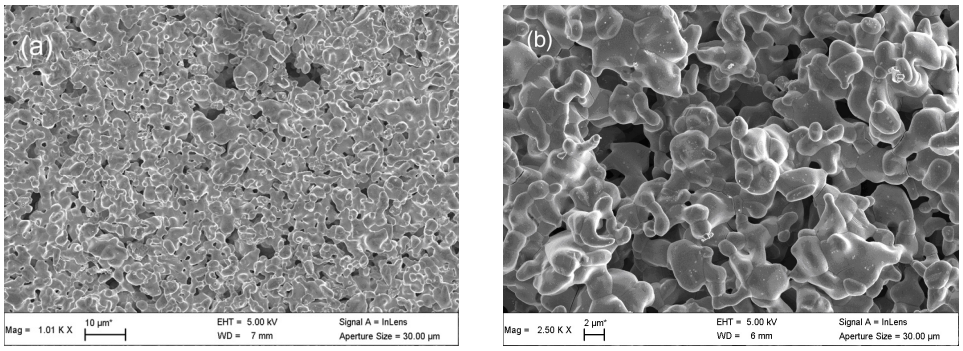

Figure 4. SEM images of the $YBaCo_4O_7$ electrode's surface before electrochemical oxidation/reduction at 1000x(a) and 5000x(b) magnification

Based on all information presented above we are presenting a mechanism for Co (II) to Co (III) global oxidation process in neutral aqueous solution in Fig. 5.

This way the oxygen activity in the superficial layer becomes more pronounced than oxygen activity in the bulk of mixed oxide. This activity gradient determines to the oxygen diffusion from the surface of Y-114 compound into the mass of mixed oxide. Oxygen diffusion rate is much lower in comparison with charge transfer or hydroxyl ions diffusion from the electrolyte solution to the electrode surface.

Therefore, the electrochemical oxidation of Co (II) to Co (III) actually consists in oxygen insertion into the crystalline structure of $YBaCo_4O_7$. Consequently, during oxidation the crystalline network of Y-114 mixed oxide becomes more compact (dense), so that oxygen diffusion is slower. Furthermore, the oxidation process of Co (II) to Co(III) is not complete.

The constriction of the mixed oxide layer induces a slight irreversible character to the oxidation of Co (II) ions, which leads to the disappearance of the oxidation plateau (3) and also to the attenuation of the reduction peak (6) in comparison with the oxidation peak (Fig. 1).

According with the presented mechanism, at anodic polarization, after the OCP, the oxidation process is controlled by the charge transfer step; this is supported by the electrochemical impedance spectra.

The electrochemical impedance spectra recorded for the $YBaCo_4O_7$ electrode during oxidation at E = 0.3 V in neutral solution are given in Fig.6.

The experimental complex plane plots show distinct features depending on the frequency range. Thus, the final part of an incomplete semicircle can be observed at high frequencies, between 100 kHz and 30.9 kHz, which is related to a charge transfer process. A slightly curved line related to a Gerischer element appears at intermediate frequencies, between 30.9 kHz and 141 Hz. Finally, a large semicircle is observed at low frequencies, between 141 Hz and 1 mHz.

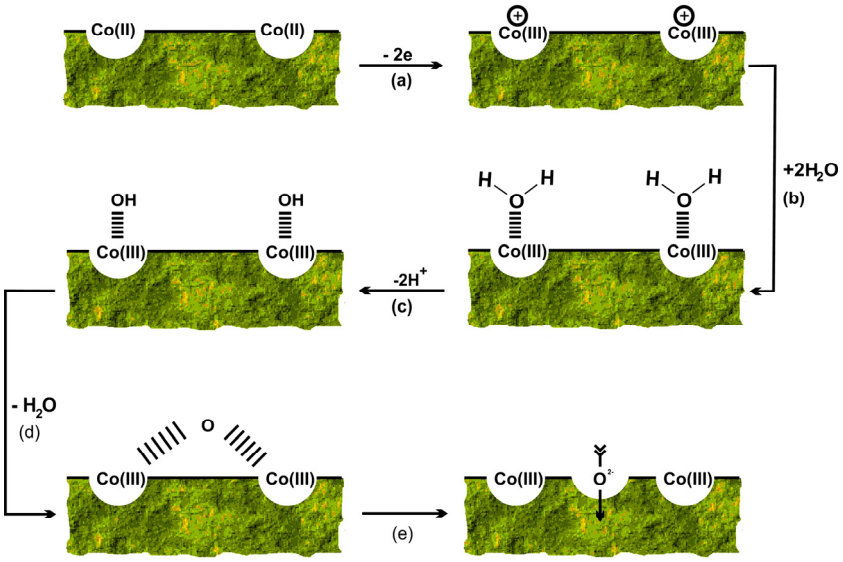

Figure 5. Proposed mechanism for the electrochemical oxidation of $YBaCo_4O_7$ in neutral solutions:

a) oxidation of Co^{2+} ions at electrode interface;
b) addition of water molecules at newly formed Co^{3+} cations;
c) elimination of H^+ ions;
d) elimination of H_2O and structural rearrangement of $YBaCo_4O_7$;
e) diffusion of oxygen ions; *lines*- preponderant ionic interaction.

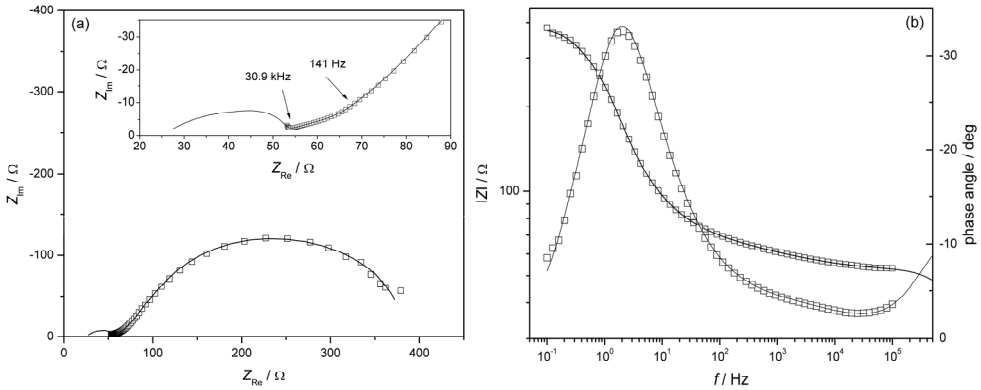

Figure 6. Experimental Nyquist (a) and Bode (b) plots for $YBaCo_4O_7$ at E = 0.3 V in 0.5 mol L^{-1} Na_2SO_4. Inset: enlargement of the medium to high frequency domain. Open symbols are experimental points and continuous lines are simulated by the CNLS fitting according to the equivalent circuit.

The experimental impedance data were modelled using the equivalent circuit given in Fig. 7. It consists of an ohmic resistance R_{Ohm} in series with a parallel connection of a constant phase element (CPE) and the charge transfer resistance R_{ct} followed by a Gerischer element (GE) and a parallel connection of a Warburg element (W) and a resistance (R) in series with a capacitor (C).

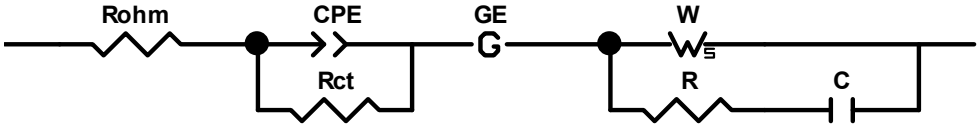

Figure 7. Equivalent electric circuit for modelling oxygen insertion into the $YBaCo_4O_7$ electrode in neutral solution.

The ohmic resistance includes the uncompensated solution resistance and a contribution from the resistance of the $YBaCo_4O_7$ electrode. The constant phase element replaces the double layer capacitance since it has been observed that it describes more accurately the behaviour of real electrochemical systems. The Gerischer element [13] is a diffusion element, similar to the Warburg impedance, which has been proposed to describe the alternating current response of an electrochemical system where a chemical reaction is preceding or following the electrochemical reaction. In its most simple form the impedance of a Gerischer element is given by:

$$Z_{GE} = Z_0 / (k + j\omega)^{1/2}$$

where Z_0 is the magnitude of the impedance at ω = 1 rad s^{-1} and k is a rate constant parameter.

The experimental impedance data were fitted to the equivalent circuit using a complex non-linear least squares procedure. The results of the fitting are shown as continuous lines in Fig. 6 and the corresponding values of the circuit elements, together with their standard errors are given in Table 2.

The high frequency part of the impedance spectra could be fitted only if the ohmic resistance was imposed to a fixed value. However, if the proposed model is used to simulate the response at high frequencies up to 10^8 Hz the whole semicircle is visible as a continuous line in the inset of Fig. 6a. The constant phase angle parameter n has a value of 0.52 and is considered to be related to surface inhomogeneities and porosity of the electrode. Values around 0.9 are common for metal electrodes, while lower values of 0.6 have been reported for porous electrodes [14].

Table 2. Experimental values of the circuit elements during oxidation of $YBaCo_4O_7$ in neutral solution

Parameter	Value
R_{Ohm} [Ω]	25 (fixed)
T [F s^{n-1}]	$7.04 \times 10^{-4} \pm 2.54 \times 10^{-4}$
n	0.52 ± 0.04
R_{ct} [Ω]	10.07 ± 0.89
Z_0 [Ω $s^{1/2}$]	$0.00344 \pm 6.2 \times 10^{-5}$
k [s^{-1}]	1.72 ± 0.03
R_W [Ω]	126.0 ± 2.2
τ_D [s]	$1.855 \times 10^{-6} \pm 0.185 \times 10^{-6}$
ϕ	0.5 (fixed)
R [Ω]	34.57 ± 0.71
C [F]	$9.06 \times 10^{-4} \pm 0.17 \times 10^{-4}$

CONCLUSIONS

Results obtained by cyclic voltammetry in neutral aqueous solution showed that the $YBaCo_4O_7$ mixed oxide is sensitive to anodic or cathodic polarization. Based on the experimental data we can conclude that the electrochemical oxidation of Co(II) ions consist in oxygen insertion in the mixed oxide structure. Because of that during oxidation the Y-114 crystalline network becomes denser, so that oxygen diffusion rate is lowered.

The compaction of Y-114 during oxidation imposes a partial irreversible character of this process, and as a consequence the oxidation leads to disappearance of the oxidation plateau and also to the attenuation of the reduction peak.

Based on the EIS spectra and the presented mechanism, the oxidation process is controlled by the charge transfer step. Thus, a complete structural characterization of the fully oxidized phase will be discussed in a forthcoming paper.

EXPERIMENTAL SECTION

The $YBaCo_4O_7$ compound was obtained using a solid state reaction, by mixing the precursor Y_2O_3, $BaCO_3$ and $CoO_{4/3}$ according to the stoichiometric cation ratio. After decarbonisation at 1000°C the powder was pressed in bars (2x2x10 mm). The bars were fired in air for 48h at 1200°C and then removed rapidly from furnace and set to ambient temperature. [1,3,4,6,12].

The electrochemical measurements were carried out using an Autolab PGSTAT 302N equipped with electrochemical impedance spectroscopy (EIS) module. The electrochemical cell was a conventional one-compartment, three-electrode glass cell with a volume of 50 mL. Two graphite counter electrodes were placed symmetrically next to the working electrode made of $YBaCo_4O_7$ pressed bar and a Ag/AgCl(sat) electrode was used as reference. All potentials in this work are given versus the reference electrode. All electrochemical measurements were performed in 0.5 mol L^{-1} Na_2SO_4 electrolyte solution. Electrochemical impedance spectroscopy measurements were carried out using the FRA module of Autolab 302N, in the frequency range from 0.1 Hz to 100 kHz and AC voltage amplitude of 10 mV. For each spectrum 60 points were collected, with a logarithmic distribution of 10 points per decade. The experimental electrochemical impedance data were fitted to the electrical equivalent circuit by a complex non-linear least squares (CNLS) Levenberg – Marquardt procedure using ZView – Scribner Associates Inc. software.

The surface area was determined according to the Brunauer-Emmet-Teller (BET) method using a ASAP 2020 M (Micromeritics Instrument Corporation USA).

REFERENCES

1. E.V. Tsipis, D.D. Khalyavin, S.V. Shiryaev, K.S. Redkina, P. Núñez, *Materials Chemistry and Physics*, **2005**, *92*, 33.
2. H. Hao, J. Cui, C. Chen, L. Pan, J. Hu, X. Hu, *Solid State Ionics,* **2006**, *177*, 631.
3. H. Haoshan, Z. Limin, H Jie, H. Xing, H Hongwei, *Journal of Rare Earths*, **2009**, *27*, 815.
4. E.V. Tsipis, V.V. Kharton, J.R. Frade, P. Núñez, *Journal of Solid State Electrochemistry*, **2005**, *9*, 547.
5. K. Zhang, Z. Zhu, R. Ran, Z Shao, V.V. Jin, S. Liu, *Journal of Alloys and Compounds*, **2010**, *492*, 552.
6. M. Valldor, M. Andersson, *Solid State Science*, **2002**, *4*, 923.
7. M. Valldor, *Solid State Science*, **2004**, *6*, 251.
8. M. Dan, V. Pralong, N. Vaszilcsin, A. Kellenberger, N. Duteanu, *Journal of Solid State Electrochemistry*, published online, DOI 10.1007/s10008-010-1189-3.
9. J.C. Grenier, A. Wattiaux, J.P. Doumerc, P. Dordor, L. Fournes, J.P. Chaminade, M. Pouchard, *Journal of Solid State Chemistry*, **1992**, *96*, 20.
10. J.C. Grenier, J.M. Bassat, J. P. Doumerc, J. Etourneau, Z. Fang, L Fournes, S. Petit, M. Pouchard, A. Wattiaux, *Journal of Materials Chemistry*, **1999**, *9*, 25.
11. K.M. Ismail, W.A. Badawy, *Journal of Applied Electrochemistry*, **2000**, *30*, 1303.
12. M.D. Levi, H. Gizbar, E. Lancry, Y. Gofer, E Levi, D. Aurbach, *Journal of Electroanalytical Chemistry*, **2004**, *569*, 211.
13. H. Gerischer, *Zeitschrift für Physikalische Chemie*, **1951**, *198*, 216.
14. A. Kellenberger, N. Vaszilcsin, W. Brandl, *Journal of Solid State Electrochemistry*, **2007**, *11*, 84.